











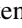

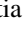



## Natural-linewidth measurements of the 3C and 3D soft-x-ray transitions in Ni XIX

Chintan Shah <sup>1,2,3,\*</sup> Steffen Kühn<sup>2,4</sup> Sonja Bernitt <sup>2,5,6,7</sup> René Steinbrügge <sup>8</sup> Moto Togawa<sup>2,4</sup> Lukas Berger <sup>2</sup>  
 Jens Buck <sup>9</sup> Moritz Hoesch <sup>8</sup> Jörn Seltmann <sup>8</sup> Mikhail G. Kozlov <sup>10</sup> Sergey G. Porsev <sup>11</sup> Ming Feng Gu <sup>12</sup>  
 F. Scott Porter <sup>1</sup> Thomas Pfeifer <sup>2</sup> Maurice A. Leutenegger <sup>1</sup> Charles Cheung <sup>11</sup>  
 Marianna S. Safronova <sup>11</sup> and José R. Crespo López-Urrutia <sup>2</sup>

<sup>1</sup>NASA *Goddard Space Flight Center*, 8800 Greenbelt Road, Greenbelt, Maryland 20771, USA

<sup>2</sup>Max-Planck-Institut für Kernphysik, Saupfercheckweg 1, 69117 Heidelberg, Germany

<sup>3</sup>Department of Physics and Astronomy, Johns Hopkins University, Baltimore, Maryland 21218, USA

<sup>4</sup>Heidelberg Graduate School of Fundamental Physics, Ruprecht-Karls-Universität Heidelberg,  
 Im Neuenheimer Feld 226, 69120 Heidelberg, Germany

<sup>5</sup>Institut für Optik und Quantenelektronik, Friedrich-Schiller-Universität Jena, Max-Wien-Platz 1, 07743 Jena, Germany

<sup>6</sup>Helmholtz-Institut Jena, Fröbelstieg 3, 07743 Jena, Germany

<sup>7</sup>GSI Helmholtzzentrum für Schwerionenforschung, Planckstraße 1, 64291 Darmstadt, Germany

<sup>8</sup>DESY, Notkestraße 85, 22607 Hamburg, Germany

<sup>9</sup>Institut für Experimentelle und Angewandte Physik, Christian-Albrechts-Universität zu Kiel, Leibnizstrasse 11-19, 24098 Kiel, Germany

<sup>10</sup>St. Petersburg Electrotechnical University “LETI,” Prof. Popov Street 5, St. Petersburg 197376, Russia

<sup>11</sup>Department of Physics and Astronomy, University of Delaware, Newark, Delaware 19716, USA

<sup>12</sup>Space Science Laboratory, University of California, Berkeley, California 94720, USA



(Received 11 April 2024; accepted 15 May 2024; published 10 June 2024)

We used the monochromatic soft-x-ray beamline P04 at the synchrotron-radiation facility PETRA III to resonantly excite the strongest  $2p$ - $3d$  transitions in neonlike Ni XIX ions,  $[2p^6]_{J=0} \rightarrow [(2p^5)_{1/2} 3d_{3/2}]_{J=1}$  and  $[2p^6]_{J=0} \rightarrow [(2p^5)_{3/2} 3d_{5/2}]_{J=1}$ , respectively dubbed 3C and 3D, achieving a resolving power of 15 000 and signal-to-background ratio of 30. We obtain their natural linewidths, with an accuracy of better than 10%, as well as the oscillator-strength ratio  $f(3C)/f(3D) = 2.51(11)$  from analysis of the resonant fluorescence spectra. These results agree with those of previous experiments, earlier predictions, and our own advanced calculations.

DOI: [10.1103/PhysRevA.109.063108](https://doi.org/10.1103/PhysRevA.109.063108)

## I. INTRODUCTION

Because of their closed-shell  $n = 2$  ground-state configuration, neonlike ions are prevalent in plasmas across a broad range of temperatures. Their strong spectral lines provide a wealth of diagnostic capabilities, including temperature, density, optical depth, and ultraviolet field intensity. Their spectra were extensively studied in investigations of the Sun and other celestial bodies with the Chandra and XMM-Newton observatories [1–16]. The spectrum of Fe XVII is the most commonly studied in the soft-x-ray band due to the high cosmic abundance of iron and the easily accessible energy of its  $n = 2$ – $3$  transitions, while Ni XIX is the second most abundant such species.

Despite the apparent simplicity of their electronic structure, systematic discrepancies in the intensities of their

strongest emission lines have long been noted between theory, astrophysical observations, and laboratory measurements (see [17] and references therein). Recently, we solved for Ne-like Fe XVII a problem that persisted for several decades: the oscillator-strength ratio between its  $2p$ - $3d$  resonance (3C:  $[2p^6]_{J=0} \rightarrow [(2p^5)_{1/2} 3d_{3/2}]_{J=1}$ ) and intercombination (3D:  $[2p^6]_{J=0} \rightarrow [(2p^5)_{3/2} 3d_{5/2}]_{J=1}$ ) lines consistently deviated from predictions [17]. Previous experiments on this topic suffered from both known and unexpected systematic uncertainties [18–30]. Our resonant excitation scheme using synchrotron radiation with a much higher resolution and signal-to-noise ratio finally brought experiment and theory into agreement [31].

In most measurements of Fe XVII, an inner-shell satellite from Na-like ions (line C:  $[2p^6 3s]_{J=1/2} \rightarrow [(2p^5)_{1/2} (3s 3d)_{5/2}]_{J=3/2}$ ) blended with the Ne-like line 3D, leading to potential systematic errors in the line ratio [20]. Experiments in which 3C and 3D were excited by electron impact and which had sufficient spectral resolving power to detect other lines of Na-like Fe allowed correction of the strength of line 3D for contamination from line C, as well as optimization of the experimental conditions to minimize production of that undesired charge state. Photoexcitation measurements suffer from a second, subtler effect: the strong autoionizing branch of the upper level of line C continuously

\*Corresponding author: [chintan.shah@mpi-hd.mpg.de](mailto:chintan.shah@mpi-hd.mpg.de)

Published by the American Physical Society under the terms of the [Creative Commons Attribution 4.0 International](https://creativecommons.org/licenses/by/4.0/) license. Further distribution of this work must maintain attribution to the author(s) and the published article's title, journal citation, and DOI. Open access publication funded by Max Planck Society.

feeds the Ne-like ground state. In these experiments with insufficient resolution to split lines  $C$  and  $3D$ , the resulting population transfer severely affected the apparent  $3C/3D$  line-intensity ratio [32]. Only the most recent photoexcitation measurements mentioned above [31], with a resolving power of 20 000, could reduce these detrimental transfer effects, reducing the effective overlap between lines  $C$  and  $3D$  to less than 1%.

Another approach to understanding issues with the  $3C/3D$  ratio in Ne-like iron is to study the same ratio along the isoelectronic sequence as a function of the atomic number  $Z$ . This has two advantages: first, any systematic errors peculiar to a single experiment are revealed as outliers; second, the scaling with the atomic number of any deviation from predictions can guide future theoretical investigations. The  $3C/3D$  ratios for Ne-like ions ranging from Cr xv to Kr xxvii ( $Z = 24\text{--}36$ ) were measured at the Lawrence Livermore National Laboratory using an electron-beam ion trap (EBIT) equipped with crystal spectrometers [20], showing systematic departures from theory of 10%–20%. Extending our photoexcitation experiment to Ne-like Ni, where lines  $3D$  and  $C$  are much farther apart than in Fe xvii, would fully suppress the undesired  $3D\text{--}C$  overlap. This, the closeness of nickel to iron in  $Z$ , and the astrophysical importance of nickel motivated our present measurement in Ne-like Ni xix ions. Because of the lower chemical abundance of nickel, its  $L$ -shell lines are weaker than those of iron in astrophysical sources. Ni xix is, nevertheless, extremely useful for understanding the spectra of the solar and stellar coronae [33,34] and for determinations of abundances, as well as plasma temperature and density [35]. In many high-energy-density plasmas [36–38],  $3C$  and  $3D$  are stronger than the other  $L$ -shell transitions and affect the Rosseland mean opacity, for which recent studies at temperatures akin to stellar interiors disagreed by 10%–20% from models for Ni [39]. Thus, an experimental benchmark is also needed for validating the underlying atomic data in opacity models and could help to clarify the iron-opacity problem [40,41].

The ability of atomic methods to accurately predict core parameters, such as transition energies and transition rates, and subsequently derived values, e.g., collisional cross sections, critically depends on the benchmark tests in which predicted values are compared against the experiment. The most readily accessible properties are transition energies, for which the most accurate experimental data can be obtained. Comparing theoretical and experimental energies is an excellent start to testing the atomic methods, as discrepancies in the energies immediately point to the method deficiencies. However, the agreement of the energies does not predict a high level of accuracy of all the other properties. Energy comparisons do not account for different dependences of the atomic properties on the distance from the nucleus, additional correlation corrections specific to the transition operators, and subtler effects of the configuration mixing. Thus, to fully validate atomic structure calculations, experiments measuring natural linewidths and lifetimes are essential.

Lifetimes of excited highly charged ions (HCIs) from the optical to the x-ray domain have been measured for decades using, among other things, accelerators, storage rings, and EBITs. At accelerators, beam-foil techniques cover a range

of a few nanoseconds to hundreds of femtoseconds [42–44], relying on spatially resolving x-ray emission following the passage of a fast ion through a thin foil. However, complexities arising from multiple excitations and the charge-state distribution limit, in general, the accuracy of such data. Kingdon traps were also used for some lifetime measurements on ions [45–47]. Storage rings have allowed for many accurate lifetime studies up to the range of seconds, e.g., in Refs. [48–58] upon injection of excited HCIs from external sources [59,60] and in the optical range also using reexcitation of the circulating ions with lasers [61–63]. In EBITs, lifetimes ranging from milliseconds down to nanoseconds are accurately measured by monitoring the decay of fluorescence after pulsed excitation, yielding uncertainties as low as 0.15% [64–68]. For the femtosecond range, natural linewidths were accessed with high-resolution crystal spectrometers using stand-alone EBITs [38] or combined with synchrotron-radiation excitation [69–71]. However, modeling line profiles remains difficult, substantially limiting the achievable accuracy.

In this paper, we present resonant photoexcitation of trapped Ni xix ions at the monochromator beamline P04 at the PETRA III facility, with a focus on the two strong emission lines,  $3C$  and  $3D$ . Several experimental improvements increased our resolving power to  $\sim 15\,000$  and the signal-to-noise ratio to  $\sim 30$ , enabling accurate determination of the  $3C/3D$  oscillator-strength ratio with approximate statistical and total uncertainties of 0.5% and 4.5%, respectively. Our observed line shapes yield the absolute natural linewidths, lifetimes, and oscillator strengths for the  $3C$  and  $3D$  lines with an accuracy better than 10%. All measurements agree well with our predictions.

## II. MEASUREMENTS AND ANALYSIS

We carried out the experiment with PolarX-EBIT [72], which is dedicated to the study of interactions of trapped HCIs with photons from external sources, at the P04 beamline [73] of the PETRA III synchrotron-radiation facility. An off-axis electron gun emits a nearly monoenergetic electron beam that is compressed to a diameter of less than  $100\ \mu\text{m}$  by an 870-mT magnetic field generated by an array of permanent magnets. Precursor atoms of Ni were brought in as a tenuous molecular beam of nickelocene [bis(cyclopentadienyl)nickel,  $(\text{C}_5\text{H}_5)_2\text{Ni}$ ] injected into the trap region through a two-stage differential pumping system. Successive electron impacts ionize Ni atoms to the charge state of choice. The ions are confined radially by the negative space-charge potential produced by the  $\sim 5.5\text{-mA}$  and  $\sim 1.1\text{-keV}$  electron beam and axially by the  $\sim 10\text{-V}$  potential difference given to the drift tubes before and after the central one. At the soft-x-ray beamline P04, an APPLE II undulator generates circularly polarized photons which are monochromatized with a variable-line-spacing platinum-coated 1200 lines/mm grating [73]. A Kirkpatrick-Baez mirror system refocuses the photon beam at the position of the PolarX trap region a few meters downstream. The focus diameter there is slightly smaller than the ion cloud itself, which is approximately  $200\ \mu\text{m}$  wide. The photon beam enters PolarX from the side where the off-axis electron gun is mounted and propagates along its longitudinal axis, defined by

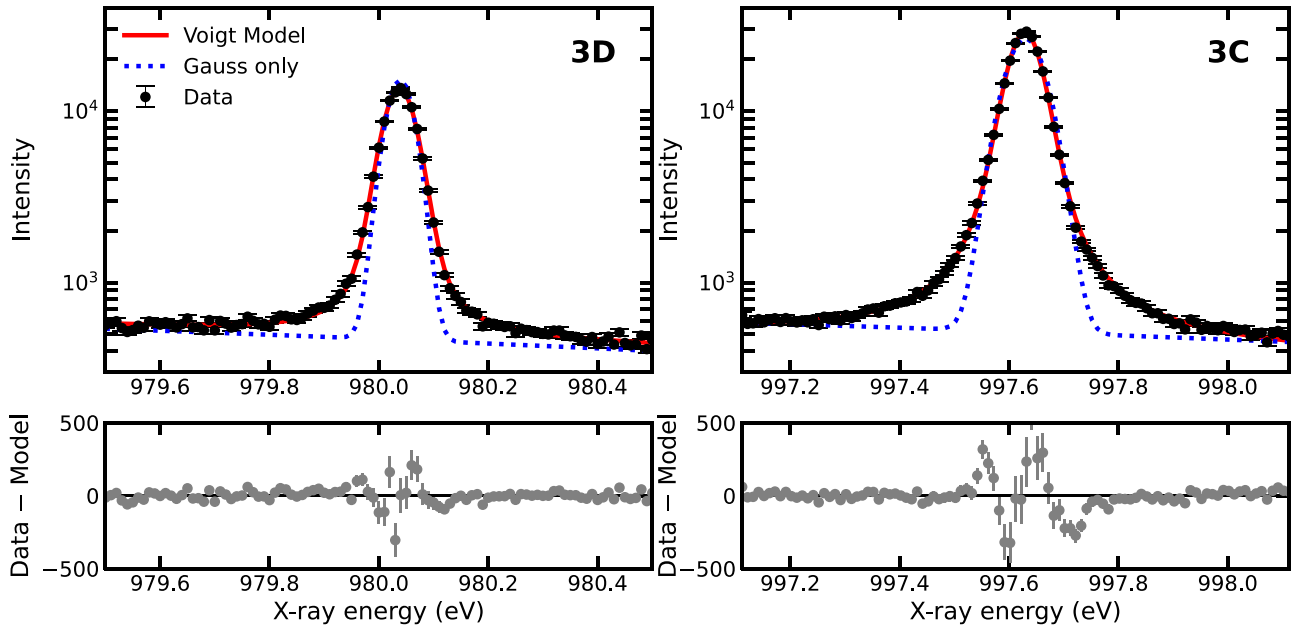


FIG. 1. Summed fluorescence yield of the 3C and 3D soft-x-ray transitions of Ni XIX versus excitation photon energy. Fitted Voigt profiles are shown in red, with their residuals in the bottom panels. A slight asymmetry of the peak causes the residuals near the center of the peak to deviate from zero. For comparison, blue curves show only the Gaussian component of the model, normalized to the same peak intensity.

the magnetic field and the narrow electron beam that it guides and compresses. The photon beam is focused for maximum overlap onto the approximately 16-mm-long cloud of Ni ions confined within the central trap electrode. Upon excitation, the resulting fluorescence is detected by two identical silicon drift detectors (SDDs) with a resolving power of 10% at 1 keV mounted at right angles to the photon beam on the top and the side of the trapping region. After passing the trap region, the photon beam exits PolarX unimpeded through its collector and enters a downstream beamline, where we measure its intensity.

For production of Ni XIX ions, the electron-beam energy must exceed 607 eV. This also leads to electron-impact-induced fluorescence from dielectronic recombination as well as resonant and direct excitation [26] that is much stronger than the sought-after photoexcitation signal. We address this by periodically switching within a few microseconds the electron-beam energy between two optimized values, breeding Ni XIX ions at 1090 eV for 200 ms and detecting their fluorescence at 280 eV for 50 ms. This suppresses in-band background photons induced by electron-impact processes, resulting in a cleaner photoexcitation signal [31]. The residual background results from electron impact production of few-hundred-eV photons which partly blend in the SDD with 3C and 3D due to its finite energy resolution and the width of the region of interest. Optimization of the ion-breeding duty cycle allowed us to further narrow the monochromator exit slit width to 25  $\mu\text{m}$  while keeping a strong fluorescence signal and achieving a robust signal-to-background ratio close to  $\sim 30$ . The narrow slit allows the resolving power of the monochromator to reach values up to 15 000 for the Ni XIX 3C and 3D transitions.

We scanned a range of  $\pm 500$  meV around the known centroid energies [35,74] in 100 steps of 10 meV each

while integrating the photoexcitation signal for  $\sim 6$  s at each monochromator step to ensure sufficient statistics in the line wings. To generate the spectrum, x rays detected within a given region of interest centered on the expected energies of 3C and 3D were summed and projected onto the monochromator energy axis. These scans were repeated 20 times, and the resulting (summed) data are shown in Fig. 1. Each individual scan is fitted with a Voigt profile, a convolution of Gaussian and Lorentzian distributions. The Gaussian component arises from the Doppler width of the trapped ions and the apparatus profile of the monochromator [75]. Meanwhile, the Lorentzian component, as explained in detail in our previous work [31,76], results not only from the natural linewidth of the transitions but also from a pseudo-Lorentzian instrumental component caused by x-ray diffraction at beamline components [77]. Total intensities were determined from the area under the curve, derived through a maximum-likelihood fit of Voigt profiles using the Cash statistic [78,79]. Furthermore, 3C and 3D intensities were corrected for the presence of a 500-nm Al filter in front of SDDs and normalized by the photon flux measured downstream of the EBIT with a calibrated photodiode, which together increase the ratio by 0.5%. Given that the intensity of the 3C and 3D transitions excited by the monochromatic x-ray beam is directly proportional to the oscillator strength of each transition [27,80], we derived an oscillator strength ratio of 2.51(2) from the measured intensities. We note that the inner-shell satellite C of the Na-like ion, previously a major source of systematic uncertainties in many experiments on Fe XVII, does not affect the Ni XIX 3C/3D line ratio. This is primarily because line C is clearly separated from line 3D, falling well outside the scan range we used. From our low-resolution measurement with a 1-mm exit slit, we determined the difference  $\Delta E_{3D-C} \approx 2.4$  eV.

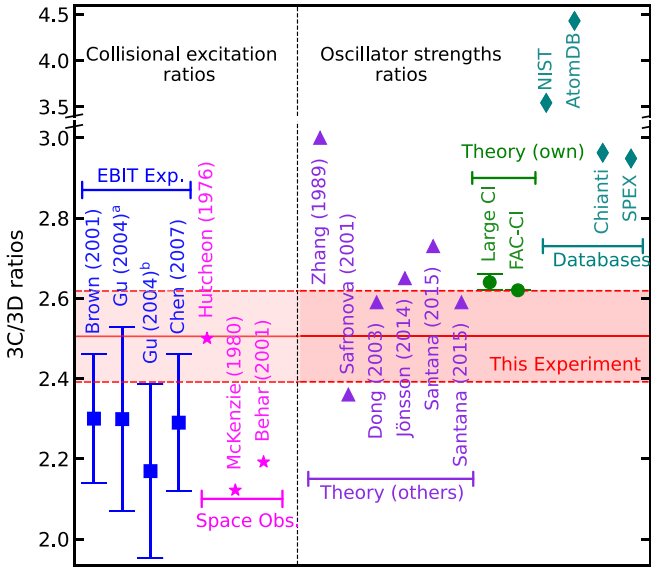


FIG. 2. Present experimental Ni XIX  $3C/3D$  oscillator-strength ratio in comparison with collision-strength ratios measured in prior EBIT experiments: experiments with a crystal spectrometer in Brown *et al.* [20], with a grating spectrometer in Gu *et al.* [35] (denoted with a superscript a), and with microcalorimeters in Gu *et al.* [35] (denoted with a superscript b) and Chen *et al.* [83]; solar observations [34,84]; and Chandra studies of Capella [7]. Our measured oscillator-strength ratio is also compared with earlier theoretical studies [85–89], our own predictions [90,91], and commonly used spectral plasma models and databases [92–95].

The measured line ratio can be affected by periodic fluctuations of the actual photon energy around its nominal value, stemming from incorrect interpolation tables for the grating and mirror angular encoders [77,81] of the monochromator, as discussed in our previous work [31,76]. To avoid this issue in subsequent works, we simultaneously measured a proxy for the fluctuations of the true photon energy with a photoelectron-energy spectrometer Angular Spectrometer for Photoelectrons with High Energy REsolution (ASPHERE) [82]. Unfortunately, this instrument was not available during the present measurements, but in follow-up campaigns [76] we found with it oscillating differences between nominal and true photon energies of up to  $\approx \pm 70$  meV in the Ni XIX  $3C$  and  $3D$  scan range. We simulated such monochromator fluctuations with mock  $3C$  and  $3D$  Voigt profiles, resulting in systematic uncertainties of approximately 3% in the  $3C/3D$  intensity ratio. A slight line-profile asymmetry caused by x-ray diffraction at beamline components was quantified by fitting with skewed Voigt profiles, showing changes in the ratio of less than 0.5%. We observed scan-to-scan variations in the amplitudes of  $3C$  and  $3D$  of  $\sim 3\%$  which are not attributable to any known cause and which we therefore take as a term in our systematic error budget. All above systematic uncertainties, including the  $\sim 0.1\%$  uncertainty in the  $3C/3D$  ratio arising from a 10% uncertainty in the thickness of the 500-nm Al optical filter, are taken into account in the final error budget for the inferred oscillator-strength ratio, namely,  $f(3C/3D) = 2.51(2)_{\text{stat}}(11)_{\text{sys}}$ , as displayed in Fig. 2. Note that the circular polarization of the photon beam does

TABLE I. Natural linewidths  $\Gamma^{\text{exp}}$  for  $3C$  and  $3D$  of Ni XIX determined using two different methods, as well as their mean. Pearson correlation coefficients  $\rho_{3C,3D}$  for  $\Gamma_{3C}$  and  $\Gamma_{3D}$  are also listed

Natural linewidths $\Gamma^{\text{exp}}$	Line $3C$ (meV)	Line $3D$ (meV)	$\rho_{3C,3D}$
Method 1	$19.8 \pm 1.2$	$7.1 \pm 1.0$	0.10
Method 2	$21.2 \pm 2.7$	$8.3 \pm 1.2$	0.94
Mean (equal weights)	$20.5 \pm 1.7$	$7.7 \pm 0.7$	0.63

not influence the ratio, as both transitions  $3C$  and  $3D$  have identical angular emission characteristics (see Appendix A in Ref. [71]).

To determine the natural linewidths of  $3C$  and  $3D$ , we used the Gaussian and Lorentzian widths extracted through Voigt fits to 20 scans of  $3C$  and  $3D$ . While Gaussian widths of approximately 50 meV for  $3C$  and  $3D$  were consistent with the experimental conditions, the extracted Lorentzian widths of  $\sim 30$  and  $\sim 17$  meV for  $3C$  and  $3D$  transitions, respectively, were clearly larger than expected from theory. We attribute this discrepancy to an additional pseudo-Lorentzian component induced by x-ray diffraction at beamline components [77,81] that artificially raises the apparent Lorentzian linewidth of observed transitions, as shown in our previous work [31]. We checked that here by measuring the  $K\alpha$ ,  $K\beta$ , and  $K\gamma$  x-ray transitions from heliumlike F VII and Ne IX several times. Their theoretical natural linewidths were taken from the NIST Atomic Spectral Database (ASD) [92,96,97], and we assigned them a conservative 10% uncertainty [35]. As Lorentzian contributions add linearly, in contrast to the quadratic addition of Gaussian widths, we subtracted the theoretical natural linewidths from the Lorentzian linewidths inferred from the measurements. We noticed an increase in the pseudo-Lorentzian beamline component dependent on the monochromator energy, which we model empirically as a quadratic function, determining the beamline Lorentzian contribution at  $3D$  and  $3C$  line energies to be 10.0(1.0) and 10.3(1.1) meV, respectively. We also derived beamline Lorentzian contributions of 7.2(5) and 7.4(5) meV at Fe XVII  $3D$  and  $3C$  energies, respectively, and upon comparison with the 7.0(3) meV obtained in our earlier work [31], which relied exclusively on the single F VIII  $K\beta$  line, we find reasonably good agreement between the present work and Kühn *et al.* [31].

To derive the natural linewidths of Ni XIX  $3C$  and  $3D$ , we subtracted the pseudo-Lorentzian instrumental component from the Lorentzian widths obtained from Voigt fits to each scan of both lines. The determined natural linewidths were 19.8(1.2) and 7.1(1.0) meV for  $3C$  and  $3D$ , respectively, indicated as method 1 in Table I and Fig. 3. Their uncertainties include the statistical error on individual widths obtained from the fit and systematic uncertainties from asymmetric line shapes (2%) and monochromator energy fluctuations at  $3C$  (2.2%) and  $3D$  (2.3%) and at the heliumlike  $K$ -shell reference transitions of heliumlike F and Ne ions (6%).

Alternatively, we can use the following equations to determine the individual natural linewidths of  $3C$  and  $3D$  using the *difference* in their uncalibrated Lorentzian widths, as shown

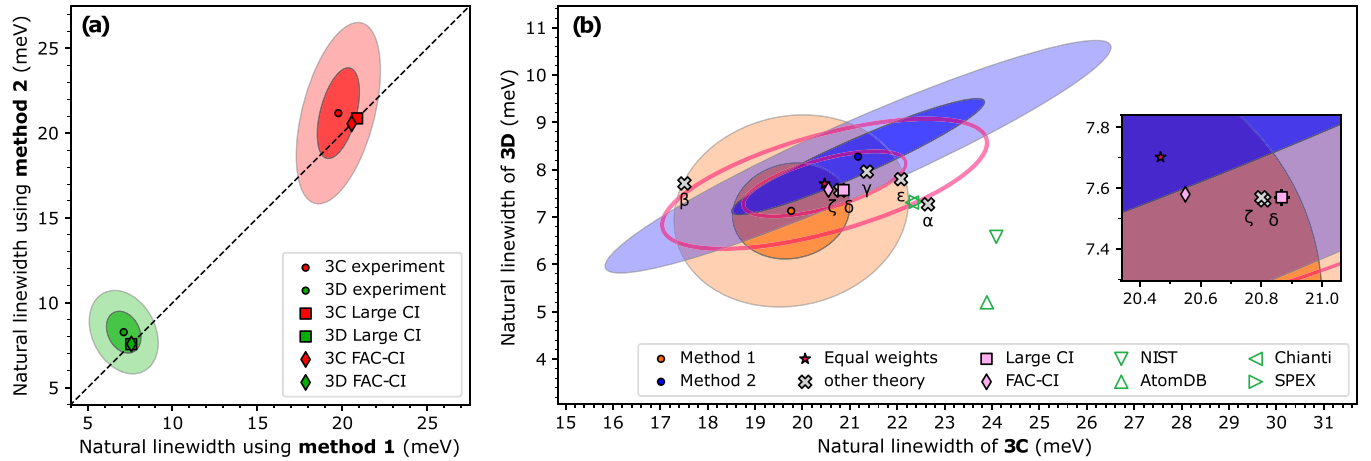


FIG. 3. (a) Results for the natural linewidths of 3C (red) and 3D (green) for Ni XIX analyzed using two different methods, with ellipses displaying their  $1\sigma$  and  $2\sigma$  experimental uncertainties. The dashed diagonal line marks where the two methods coincide. Predictions from large-scale configuration interaction (large-CI; squares) and Flexible Atomic Code Configuration Interaction (FAC-CI) method (diamonds) are shown. (b) Natural linewidths inferred for 3C and 3D. Ellipses:  $1\sigma$  and  $2\sigma$  experimental uncertainties for method 1 (orange) and method 2 (blue), as well as for their mean with equal weights (magenta star and lines). Symbols: Predictions from our large-CI (pink square), our FAC-CI (pink diamond), other calculations (gray crosses:  $\alpha$  Distorted Wave (DW), Zhang and Sampson [85];  $\beta$  many-body perturbation theory (MBPT), Safronova *et al.* [86];  $\gamma$  multichannel Dirac Fock (MCDF), Dong *et al.* [87];  $\delta$  (CI), Jönsson *et al.* [88]; and  $\varepsilon$  (CI),  $\zeta$  (MBPT), Santana *et al.* [89]).

in Kühn *et al.* [31]:

$$\Gamma_{3C} = \frac{\Delta\Gamma_{3C-3D}}{1 - f(\frac{3D}{3C})E(\frac{3D}{3C})^2}, \quad \Gamma_{3D} = \frac{\Delta\Gamma_{3C-3D}}{f(\frac{3C}{3D})E(\frac{3C}{3D})^2 - 1}.$$

However, in this second method, we assume that the pseudo-Lorentzian contribution from the beamline is similar for both the 3C and 3D lines, as in Kühn *et al.* [30]. This allows the subtraction of Lorentzian widths obtained directly from the 3C and 3D Voigt fits [ $\Delta\Gamma_{3C-3D} = 13.0(1.4)$  meV]. By utilizing this difference along with the measured  $f(3C/3D)$  oscillator-strength ratio in the present work and the transition energy  $E(3C/3D)$  ratio measured in [74] in the above equations, we determine the natural linewidths of 3C and 3D to be 21.2(2.7) and 8.3(1.2) meV, respectively. The final errors in this method (method 2) account for Voigt fit statistical errors on individual widths, asymmetric line shapes (2%), and the effects of monochromator energy fluctuations on 3C (2.2%) and 3D (2.3%) and on  $\Delta\Gamma_{3C-3D}$  (5%), in addition to the uncertainty in  $f(3C/3D)$  from this work and the  $E(3C/3D)$  uncertainty from [74].

In both methods, we propagated uncertainties and covariances using Monte Carlo methods, obtaining final natural linewidths values for the 3C and 3D lines as unweighted means of all 20 individual measurements. A comparison of the results of both methods is displayed in Fig. 3(a). Figure 3(a) shows that results for both linewidths are largely uncorrelated in method 1, as it is less prone to systematics, while method 2 exhibits a Pearson correlation coefficient close to 1 for both linewidths, indicating high correlation and greater susceptibility to systematics arising from amplitude ratios, energy ratios, and the assumption of similar beamline components. Since both methods use essentially the same dataset but produce slightly different results, we use equal weighting to ensure a balanced representation of both methods for our final re-

sults presented in Table I and shown as magenta ellipses in Fig. 3(b). The mean uncertainties given in Table I are the  $1\sigma$  widths of the projections of the ellipses onto their respective natural linewidth axes as represented by the magenta ellipses in Fig. 3(b).

### III. RESULTS AND DISCUSSION

Figure 2 compares our results with earlier experimental data, observations, and predictions. Our own calculations using large-scale configuration interaction (large-CI) [90] and FAC-CI [91] methods, both accounting for the relativistic Breit interaction and quantum electrodynamics (QED) effects, yield an oscillator-strength ratio which agrees with our experiment within the uncertainties. Details of large-CI computations are given in the Appendix A. Additional comparisons with other theoretical values from the literature showed typical departures within a  $1\sigma$ – $2\sigma$  range, with the largest one being from Zhang and Sampson [85].

Three laboratory measurements of the 3C/3D intensity ratio of Ni XIX based on electron-impact excitation were reported [20,35,83]. The collisional excitation ratios from all three previous experiments span 1.90–2.35, slightly lower than the oscillator strength ratio measured in our experiment, but all four experiments are mutually consistent within uncertainties. Observations of the solar corona [34,84] and Capella [7] show some scatter in the 3C/3D ratio, but in the absence of uncertainty estimates we cannot quantify the level of agreement with laboratory measurements.

Figure 3(a) shows a comparison between measured 3C and 3D natural linewidths obtained using two different methods, which agree (see dashed diagonal lines) with each other and our predictions. Our calculations using both large-CI and FAC-CI methods agree within the  $1\sigma$  uncertainty of our experimental results. As can be seen in Fig. 3(b), the other older calculations from Zhang and Sampson [85] and Safronova

*et al.* [86] show disagreement; however, their values fall just outside of the  $2\sigma$  ellipse of mean natural linewidths, whereas somewhat recent calculations presented in Refs. [87–89] show agreement within the  $1\sigma$  ellipse.

The individual oscillator strengths of  $3C$  and  $3D$  can be derived from the natural linewidth using the relation  $f_{fi}^{\text{exp}} = C \lambda_{if}^2 (g_i/g_f) (\Gamma_{\text{exp}}/\hbar)$ , where  $C = 1/(32\pi^3 \alpha a_0^2 Ry) = 1.49919 \times 10^{-14} \text{ nm}^{-2} \text{ s}$ .  $g_i$  and  $g_f$  represent the statistical weights of the initial ( $i$ ) and final ( $f$ ) states, respectively.  $\lambda_{if}$  is the transition wavelength given in nanometers taken from [74], and  $\hbar$  is the reduced Planck constant. The experimental oscillator strengths for  $3C$  and  $3D$  are found to be  $2.17 \pm 0.18$  and  $0.84 \pm 0.08$ , respectively. This corresponds to lifetimes of  $32.11 \pm 2.68$  and  $85.48 \pm 7.84$  fs for  $3C$  and  $3D$ , respectively. All of these measured quantities agree very well with our predictions.

Our present experimental validation of oscillator strengths effectively eliminates uncertainties in atomic data as potential contributors to the observed discrepancies in nickel opacity measurements [39] and iron opacity [31,40,41]. The measured oscillator strengths offer direct application in astrophysical modeling, enabling the diagnosis of turbulent velocity in moderately optically thick plasmas [9,98]. Following a comparison with oscillator strength ratios and natural linewidths from established databases such as NIST ASD [92], AtomDB [93], Chianti [94], and SPEX [95], significant discrepancies were identified with our experimental results. There is a pressing need to update these databases with such precise measurements in view of the crucial role of accurate data in modeling observational spectra from existing missions like Chandra and XMM-Newton, as well as upcoming observations with XRISM [99], which was recently successfully launched, and future planned missions such as Athena [100], LEM [101], HUBS [102], Arcus [103], HiReX [104], and Lynx [105]. The present combination of experimental benchmark and converged calculations is a crucial consistency check for atomic data required to interpret x-ray observations in astrophysics, fusion, and high-energy density plasma research.

#### ACKNOWLEDGMENTS

This research was funded by the Max Planck Society (MPG) and the German Federal Ministry of Education and Research (BMBF) under Project No. 05K13SJ2. C.S. acknowledges support from MPG and the NASA Astrophysics Program. F.S.P. and M.A.L. acknowledge support from the NASA Astrophysics Program. The theoretical work was supported by U.S. NSF Grants No. PHY-2012068 and No. PHY-2309254, U.S. Office of Naval Research Grant No. N00014-20-1-2513, and the European Research Council (ERC) under the Horizon 2020 Research and Innovation Programme of the European Union (Grant Agreement No. 856415). Calculations were performed in part using the computing resources at the University of Delaware, in particular the Caviness and DARWIN high-performance computing clusters. This theoretical work, including M.G.K.'s contributions, was carried out as part of a scientific collaboration during the calendar year 2020. We acknowledge DESY (Hamburg, Germany), a member of the Helmholtz Association

HGF, for the provision of experimental facilities. Parts of this research were carried out at PETRA III. We thank J. Viehhaus and R. Follath for valuable discussions on x-ray monochromator resolution and performance and the synchrotron-operation team and P04 team at PETRA III for their skillful and reliable work. M.S.S. thanks MPIK, Heidelberg, for hospitality.

#### APPENDIX: THEORY

The calculations are carried out using a large-scale configuration interaction (CI) method [90], including correlations from all 10 electrons. Basis sets of increasing sizes are used to check for convergence of the values. The basis set is designated by the highest principal quantum number for each partial wave included. For example,  $[12spdfg]$  means that all orbitals up to  $n = 12$  are included for the  $spdfg$  partial waves. We begin by considering all possible single and double excitations to orbitals up to  $5spdf6g$  from the  $2s^22p^6$  and  $2s^22p^53p$  even configurations and  $2s^22p^53s$ ,  $2s^22p^53d$ , and  $2s2p^63p$  odd configurations, correlating eight electrons. We verified that inclusion of the  $2s2p^63s$  even configuration and  $2s^22p^54s$  and  $2s^22p^54d$  odd configurations as basic configurations has a negligible effect on the energies and relevant matrix elements. The calculated contributions to the energies of Ni XIX are listed in Table II. The results are compared with a revised analysis of the experimental data [106]. We use  $jj$  coupling and NIST-style  $LS$ -coupling term designations for comparisons. Contributions to the  $E1$  reduced matrix elements  $D(3D)$  and  $D(3C)$  and the  $3C/3D$  oscillator strengths ratios are listed in Table III. The  $E(3C/3D)$  energy ratio is 1.018, and the  $f(3C/3D)$  oscillator strength ratio is 2.64(2).

To assess the impact of triple excitations, we consider a broad range of configurations up to  $5spdf6g$ . As demonstrated in Tables II and III, these excitations result in negligible corrections to both energies and matrix elements. Subsequently, we expand the basis set to  $[12spdfg]$ , leading to a significant improvement in the agreement of energies with experimental values and a minimal shift in the ratio ( $-0.008$ ). Further accounting for contributions from the  $1s^2$  shell with the  $[12spdfg]$  basis improves agreement with experimental energies, albeit with a marginal contribution to the  $3C/3D$  ratio ( $-0.006$ ). A comparison of results for  $D(3C)$  and  $D(3D)$  obtained in the length and velocity gauges reveals only a marginal difference of 0.001 for the  $[12spdfg]$  basis. Expanding the basis set to  $[17spdfg]$  produces a modest improvement in energies compared to experiment, accompanied by a slight shift in the ratio ( $-0.001$ ). Further expansion to  $[22spdfg]$  results in minor corrections to energies, with an even smaller contribution to the ratio ( $-0.0005$ ). The quantum electrodynamic (QED) contributions are included following Ref. [107]. The inclusion of QED has a small effect on the individual line energies but makes a considerable contribution to the energy difference of  $3C$  and  $3D$  (see Table II). Furthermore, the ratio is changed by  $-0.01$  by accounting for QED.

Additionally, we compute the transition rates for all other transitions contributing to the radiative decay of the  $3C$  and  $3D$  levels. The sums of these rates are small and are listed in Table III. Linewidth values correspond to total transition rates,

TABLE II. Contributions to the energies of  $\text{Ni}^{18+}$  calculated with increased size basis sets and greater numbers of configurations. The results are compared with a revised analysis of the experimental data [106]. All energies are given in  $\text{cm}^{-1}$  with the exception of the last row, which shows the difference of the 3C and 3D energies in eV. The basis set is designated by the highest quantum number for each partial wave included. For example, [12spdfg] means that all orbitals up to  $n = 12$  are included for *spdfg* partial waves. Contributions from the larger basis sets [17spdfg] and [22spdfg], triple excitations, excitations from the  $1s^2$  shells, and QED contributions are given separately. The Diff. column represents the absolute difference between Expt. [106] and our “Final” predictions. Diff (%) shows this difference in relative percent.

Configuration	$J$	Expt.								Final	Diff. [106]	Diff. (%) [106]	
		[106]	[5spdf6g]	Triples	+ [12spdfg]	$1s^2$	+ [17spdfg]	+ [22spdfg]	QED				
$2p^6$	$^1S$	0	0	0	0	0	0	0	0	0	0	0	
$2p^53p$	$(3/2, 1/2)$	1	7381990	7374679	-206	3579	351	797	372	44	7379615	2375	0.03
$2p^53p$	$(3/2, 1/2)$	2	7409915	7403138	-2	2880	264	724	331	29	7407364	2551	0.03
$2p^53p$	$(3/2, 3/2)$	3	7431735	7424692	-4	3023	261	738	340	102	7429152	2583	0.03
$2p^53p$	$(3/2, 3/2)$	1	7440050	7433248	-11	2836	277	730	332	85	7437497	2553	0.03
$2p^53s$	$(3/2, 1/2)^o$	2	7105260	7096413	17	3417	478	751	350	1052	7102477	2783	0.04
$2p^53s$	$(3/2, 1/2)^o$	1	7122600	7114019	15	3303	415	722	337	1052	7119862	2738	0.04
$2p^53s$	$(1/2, 1/2)^o$	1	7247700	7249597	14	3386	498	735	345	1403	7255978	-8278	0.11
$2p^53d$	$(3/2, 3/2)^o$	1	7807700	7801245	19	2336	409	684	363	72	7805128	2572	0.03
$2p^53d$	$(3/2, 5/2)^o$	2	7825770	7819486	19	1839	415	651	359	87	7822856	2914	0.04
$2p^53d$	$(3/2, 5/2)^o$	4	7825280	7819623	19	2044	410	677	362	88	7823223	2057	0.03
$2p^53d$	$(3/2, 3/2)^o$	3	7830930	7825368	17	1687	414	633	353	81	7828554	2376	0.03
$2p^53d$	$(3/2, 3/2)^o$	2	7847100	7841657	18	1638	410	654	356	86	7844819	2281	0.03
$2p^53d$	$(3/2, 5/2)^o$	3	7857640	7852407	17	1705	407	630	350	90	7855606	2034	0.04
$2p^53d$	$(3/2, 5/2)^o$	1	7901400	7899252	3	1681	384	638	352	136	7902446	-1046	0.01
$2p^53d$	$(1/2, 3/2)^o$	2	7972475	7967013	17	1683	484	657	362	432	7970647	1828	0.02
$2p^53d$	$(1/2, 5/2)^o$	2	7980810	7975017	17	1933	475	667	362	427	7978897	1913	0.02
$2p^53d$	$(1/2, 5/2)^o$	3	7986640	7981013	16	1759	481	638	356	443	7984706	1934	0.02
$2p^53d$	$(1/2, 3/2)^o$	1	8041800	8040754	-29	1668	383	633	353	372	8044132	-2332	0.03
3C - 3D	(eV)		17.4074	17.5440	-0.0039	-0.0016	-0.0002	-0.0006	-0.0001	0.0291	17.5669		

with uncertainties computed from the largest uncertainties in the 3C and 3D matrix elements, including additional configurations in CI space and QED. Additional uncertainties due to

$h$  orbitals for transition rates and linewidths, based on recent studies of  $\text{Fe}^{16+}$  [76], are included, and the final uncertainties are computed based on the relative difference.

TABLE III. Contributions to the  $E1$  reduced matrix elements  $D(3D) = D[2p^6 \ ^1S_0 - 2p^53d \ (3/2, 5/2)]$  and  $D(3C) = D[2p^6 \ ^1S_0 - 2p^53d \ (1/2, 3/2)]$  (in a.u.) and the ratio of the respective oscillator strengths  $R$  in  $\text{Ni}^{18+}$ . See the caption of Table II for designations.  $L$  and  $V$  compare results obtained in length and velocity gauges for the [12spdfg] basis. All other results are calculated using the length gauge. The transition rates and linewidth are listed at the bottom. The total of the other transition rates contributing to the lifetimes of the 3C and 3D levels is labeled “Other transitions.”

Basis set	$D(3C)$	$\Delta D(3C)$	$D(3D)$	$\Delta D(3D)$	$R(3C/3D)$	$\Delta R$	
[5spdf6g]	0.30012		0.18530		2.670		
	+Triples	0.29999	-0.00013	0.18530	0.00000	2.668	-0.002
[12spdfg]	$L$	0.30031	0.00019	0.18568	0.00038	2.662	-0.008
	$V$	0.30060		0.18582		2.663	
[12spdfg]	+ $1s^2$	0.30018	-0.00013	0.18581	0.00013	2.656	-0.006
[17spdfg]		0.30032	0.00001	0.18571	0.00003	2.662	-0.001
[22spdfg]		0.30031	-0.00001	0.18572	0.00001	2.661	-0.0005
QED			-0.00012		0.00028		-0.010
Final		0.29993		0.18613		2.64(2)	
Recommended transition rate ( $\text{s}^{-1}$ )		$3.168(4) \times 10^{13}$		$1.148(4) \times 10^{13}$			
Other transitions ( $\text{s}^{-1}$ )		$1.75 \times 10^{10}$		$1.59 \times 10^{10}$			
Total rate ( $\text{s}^{-1}$ )		$3.170(4) \times 10^{13}$		$1.150(4) \times 10^{13}$			
Linewidth (meV)		20.867(26)		7.570(27)			

- [1] J. Parkinson, *Astron. Astrophys.* **24**, 215 (1973).
- [2] B. W. Smith, J. B. Mann, R. D. Cowan, and J. C. Raymond, *Astrophys. J.* **298**, 898 (1985).
- [3] J. T. Schmelz, J. L. R. Saba, and K. T. Strong, *Astrophys. J.* **398**, L115 (1992).
- [4] K. Waljeski, D. Moses, K. P. Dere, J. L. R. Saba, K. T. Strong, D. F. Webb, and D. M. Zarro, *Astrophys. J.* **429**, 909 (1994).
- [5] K. J. H. Phillips, C. J. Greer, A. K. Bhatia, and F. P. Keenan, *Astrophys. J. Lett.* **469**, L57 (1996).
- [6] C. W. Mauche, D. A. Liedahl, and K. B. Fournier, *Astrophys. J.* **560**, 992 (2001).
- [7] E. Behar, J. Cottam, and S. Kahn, *Astrophys. J.* **548**, 966 (2001).
- [8] R. Doron and E. Behar, *Astrophys. J.* **574**, 518 (2002).
- [9] H. Xu, S. M. Kahn, J. R. Peterson, E. Behar, F. B. S. Paerels, R. F. Mushotzky, J. G. Jernigan, A. C. Brinkman, and K. Makishima, *Astrophys. J.* **579**, 600 (2002).
- [10] M. F. Gu, *Astrophys. J.* **582**, 1241 (2003).
- [11] F. B. S. Paerels and S. M. Kahn, *Annu. Rev. Astron. Astrophys.* **41**, 291 (2003).
- [12] A. Pradhan and S. Nahar, *Atomic Astrophysics and Spectroscopy* (Cambridge University Press, Cambridge, 2011).
- [13] P. Beiersdorfer, N. Hell, and J. Lepson, *Astrophys. J.* **864**, 24 (2018).
- [14] L. Gu, A. J. J. Raassen, J. Mao, J. de Plaa, C. Shah, C. Pinto, N. Werner, A. Simionescu, F. Mernier, and J. S. Kaastra, *Astron. Astrophys.* **627**, A51 (2019).
- [15] L. Gu, C. Shah, J. Mao, T. Raassen, J. de Plaa, C. Pinto, H. Akamatsu, N. Werner, A. Simionescu, F. Mernier, M. Sawada, P. Mohanty, P. Amaro, M. F. Gu, F. S. Porter, J. R. Crespo López-Urrutia, and J. S. Kaastra, *Astron. Astrophys.* **641**, A93 (2020).
- [16] G. J. Grell, M. A. Leutenegger, and C. Shah, *Astrophys. J.* **917**, 105 (2021).
- [17] G. Brown, *Can. J. Phys.* **86**, 199 (2008).
- [18] G. Brown, P. Beiersdorfer, D. Liedahl, K. Widmann, and S. Kahn, *Astrophys. J.* **502**, 1015 (1998).
- [19] G. Brown, P. Beiersdorfer, H. Chen, M. Chen, and K. Reed, *Astrophys. J. Lett.* **557**, L75 (2001).
- [20] G. V. Brown, P. Beiersdorfer, and K. Widmann, *Phys. Rev. A* **63**, 032719 (2001).
- [21] G. V. Brown, P. Beiersdorfer, H. Chen, J. H. Scofield, K. R. Boyce, R. L. Kelley, C. A. Kilbourne, F. S. Porter, M. F. Gu, S. M. Kahn, and A. E. Szymkowiak, *Phys. Rev. Lett.* **96**, 253201 (2006).
- [22] P. Beiersdorfer *et al.*, *Astrophys. J. Lett.* **576**, L169 (2002).
- [23] J. Gillaspay, T. Lin, L. Tedesco, J. N. Tan, J. M. Pomeroy, J. Laming, N. Brickhouse, G.-X. Chen, and E. Silver, *Astrophys. J.* **728**, 132 (2011).
- [24] P. Beiersdorfer, M. Bitter, S. Von Goeler, and K. Hill, *Astrophys. J.* **610**, 616 (2004).
- [25] P. Beiersdorfer, J. K. Lepson, M. F. Gu, and M. Bitter, *Astrophys. J.* **850**, 57 (2017).
- [26] C. Shah, J. R. Crespo López-Urrutia, M. F. Gu, T. Pfeifer, J. Marques, F. Grilo, J. P. Santos, and P. Amaro, *Astrophys. J.* **881**, 100 (2019).
- [27] S. Bernitt *et al.*, *Nature (London)* **492**, 225 (2012).
- [28] N. S. Oreshkina, S. M. Cavaletto, C. H. Keitel, and Z. Harman, *Phys. Rev. Lett.* **113**, 143001 (2014).
- [29] S. D. Loch, C. P. Ballance, Y. Li, M. Fogle, and C. J. Fontes, *Astrophys. J.* **801**, L13 (2015).
- [30] S. Kühn *et al.*, *Phys. Rev. Lett.* **124**, 225001 (2020).
- [31] S. Kühn *et al.*, *Phys. Rev. Lett.* **129**, 245001 (2022).
- [32] C. Wu and X. Gao, *Sci. Rep.* **9**, 7463 (2019).
- [33] M. Loulergue and H. Nussbaumer, *Astron. Astrophys.* **45**, 125 (1975).
- [34] R. J. Hutcheon, J. P. Pye, and K. D. Evans, *Sol. Phys.* **46**, 171 (1976).
- [35] M. F. Gu, P. Beiersdorfer, G. V. Brown, H. Chen, K. R. Boyce, R. L. Kelley, C. A. Kilbourne, F. S. Porter, and S. M. Kahn, *Astrophys. J.* **607**, L143 (2004).
- [36] F. J. Rogers and C. A. Iglesias, *Science* **263**, 50 (1994).
- [37] M. J. Seaton, Y. Yan, D. Mihalas, and A. K. Pradhan, *Mon. Not. R. Astron. Soc.* **266**, 805 (1994).
- [38] P. Beiersdorfer, A. L. Osterheld, V. Decaux, and K. Widmann, *Phys. Rev. Lett.* **77**, 5353 (1996).
- [39] T. Nagayama *et al.*, *Phys. Rev. Lett.* **122**, 235001 (2019).
- [40] J. E. Bailey *et al.*, *Phys. Rev. Lett.* **99**, 265002 (2007).
- [41] C. Fontes, C. Fryer, A. Hungerford, P. Hakel, J. Colgan, D. Kilcrease, and M. Sherrill, *High Energy Density Phys.* **16**, 53 (2015).
- [42] H. D. Betz, F. Bell, H. Panke, G. Kalkoffen, M. Welz, and D. Evers, *Phys. Rev. Lett.* **33**, 807 (1974).
- [43] E. Träbert, *Phys. Scr.* **T120**, 56 (2005).
- [44] E. Träbert, *J. Phys. B* **43**, 074034 (2010).
- [45] D. P. Moehs, D. A. Church, M. I. Bhatti, and W. F. Perger, *Phys. Rev. Lett.* **85**, 38 (2000).
- [46] D. P. Moehs, M. I. Bhatti, and D. A. Church, *Phys. Rev. A* **63**, 032515 (2001).
- [47] S. J. Smith, A. Chutjian, and J. A. Lozano, *Phys. Rev. A* **72**, 062504 (2005).
- [48] S. Mannervik, J. Lidberg, L. O. Norlin, and P. Royen, *Phys. Rev. A* **56**, R1075 (1997).
- [49] E. Träbert, G. Gwinner, A. Wolf, E. J. Knystautas, H.-P. Garnir, and X. Tordoir, *J. Phys. B* **35**, 671 (2002).
- [50] E. Träbert, *Can. J. Phys.* **80**, 1481 (2002).
- [51] E. Träbert, A. G. Calamai, G. Gwinner, E. J. Knystautas, E. H. Pinnington, and A. Wolf, *J. Phys. B* **36**, 1129 (2003).
- [52] E. Träbert, G. Saathoff, and A. Wolf, *J. Phys. B* **37**, 945 (2004).
- [53] E. Träbert, S. Reinhardt, J. Hoffmann, and A. Wolf, *J. Phys. B* **39**, 945 (2006).
- [54] E. Träbert, M. Grieser, J. Hoffmann, C. Krantz, R. Repnow, and A. Wolf, *Phys. Rev. A* **85**, 042508 (2012).
- [55] E. Träbert, M. Grieser, R. von Hahn, C. Krantz, R. Repnow, and A. Wolf, *New J. Phys.* **14**, 023061 (2012).
- [56] E. Träbert, M. Grieser, C. Krantz, R. Repnow, A. Wolf, F. J. Diaz, Y. Ishikawa, and J. A. Santana, *J. Phys. B* **45**, 215003 (2012).
- [57] E. Träbert, *Atoms* **10**, 114 (2022).
- [58] E. Träbert, *Atoms* **11**, 85 (2023).
- [59] D. Habs *et al.*, *Nucl. Instrum. Methods Phys. Res., Sect. B* **43**, 390 (1989).
- [60] J. Doerfert, E. Träbert, A. Wolf, D. Schwalm, and O. Uwira, *Phys. Rev. Lett.* **78**, 4355 (1997).
- [61] I. Klaft, S. Borneis, T. Engel, B. Fricke, R. Grieser, G. Huber, T. Kühl, D. Marx, R. Neumann, S. Schröder, P. Seelig, and L. Völker, *Phys. Rev. Lett.* **73**, 2425 (1994).
- [62] P. Seelig *et al.*, *Phys. Rev. Lett.* **81**, 4824 (1998).
- [63] M. Lochmann *et al.*, *Phys. Rev. A* **90**, 030501(R) (2014).



- [64] J. R. Crespo López-Urrutia, P. Beiersdorfer, D. W. Savin, and K. Widmann, *Phys. Rev. A* **58**, 238 (1998).
- [65] P. Beiersdorfer, E. Träbert, and E. H. Pinnington, *Astrophys. J.* **587**, 836 (2003).
- [66] J. R. Crespo López-Urrutia, P. Beiersdorfer, and K. Widmann, *Phys. Rev. A* **74**, 012507 (2006).
- [67] J. R. Crespo López-Urrutia and P. Beiersdorfer, *Astrophys. J.* **721**, 576 (2010).
- [68] P. Beiersdorfer, J. R. Crespo López-Urrutia, and E. Träbert, *Astrophys. J.* **817**, 67 (2016).
- [69] J. K. Rudolph, S. Bernitt, S. W. Epp, R. Steinbrügge, C. Beilmann, G. V. Brown, S. Eberle, A. Graf, Z. Harman, N. Hell, M. Leutenegger, A. Müller, K. Schlage, H.-C. Wille, H. Yavaş, J. Ullrich, and J. R. Crespo López-Urrutia, *Phys. Rev. Lett.* **111**, 103002 (2013).
- [70] R. Steinbrügge, S. Bernitt, S. W. Epp, J. K. Rudolph, C. Beilmann, H. Bekker, S. Eberle, A. Müller, O. O. Versolato, H.-C. Wille, H. Yavaş, J. Ullrich, and J. R. Crespo López-Urrutia, *Phys. Rev. A* **91**, 032502 (2015).
- [71] R. Steinbrügge, S. Kühn, F. Nicastro, M. F. Gu, M. Togawa, M. Hoesch, J. Seltmann, I. Sergeev, F. Trinter, S. Bernitt, C. Shah, M. A. Leutenegger, and J. R. Crespo López-Urrutia, *Astrophys. J.* **941**, 188 (2022).
- [72] P. Mücke, S. Kühn, L. Buchauer, J. R. Harries, T. M. Bücking, K. Blaum, A. Cieluch, A. Egl, D. Hollain, S. Kraemer, T. Pfeifer, P. O. Schmidt, R. X. Schüssler, C. Schweiger, T. Stöhlker, S. Sturm, R. N. Wolf, S. Bernitt, and J. R. Crespo López-Urrutia, *Rev. Sci. Instrum.* **89**, 063109 (2018).
- [73] J. Viefhaus, F. Scholz, S. Deinert, L. Glaser, M. Ilchen, J. Seltmann, P. Walter, and F. Siewert, *Nucl. Instrum. Methods Phys. Res., Sect. A* **710**, 151 (2013).
- [74] M. F. Gu, P. Beiersdorfer, G. V. Brown, H. Chen, D. B. Thorn, and S. M. Kahn, *Astrophys. J.* **657**, 1172 (2007).
- [75] M. Hoesch, J. Seltmann, F. Trinter, S. Kühn, M. Togawa, R. Steinbrügge, S. Bernitt, and J. R. C. López-Urrutia, *J. Phys.: Conf. Ser.* **2380**, 012086 (2022).
- [76] C. Shah, M. Togawa, M. Botz, J. Danisch, J. J. Goes, S. Bernitt, M. Maxton, K. Köbnick, J. Buck, J. Seltmann, M. Hoesch, M. F. Gu, F. S. Porter, T. Pfeifer, M. A. Leutenegger, C. Cheung, M. S. Safronova, and J. R. Crespo López-Urrutia, [arXiv:2401.08395](https://arxiv.org/abs/2401.08395).
- [77] R. Follath and A. Balzer, in *SRI 2009, 10th International Conference on Synchrotron Radiation Instrumentation*, edited by R. Garrett, I. Gentle, K. Nugent, and S. Wilkins, AIP Conf. Ser. No. 1234 (AIP, Melville, NY, 2010), pp. 657–660.
- [78] W. Cash, *Astrophys. J.* **228**, 939 (1979).
- [79] J. S. Kaastra, *Astron. Astrophys.* **605**, A51 (2017).
- [80] E. Träbert, *Atoms* **10**, 46 (2022).
- [81] J. Krempaský, R. Follath, V. N. Strocov, T. Schmitt, and U. Flechsig, *Proc. SPIE* **8139**, 81390K (2011).
- [82] K. Rossnagel, L. Kipp, M. Skibowski, and S. Harm, *Nucl. Instrum. Methods Phys. Res., Sect. A* **467–468**, 1485 (2001).
- [83] G. X. Chen, K. Kirby, E. Silver, N. S. Brickhouse, J. D. Gillaspay, J. N. Tan, J. M. Pomeroy, and J. M. Laming, *Phys. Rev. Lett.* **97**, 143201 (2006).
- [84] D. McKenzie, P. Landecker, R. Broussard, H. Ruge, R. Young, U. Feldman, and G. Doschek, *Astrophys. J.* **241**, 409 (1980).
- [85] H. L. Zhang and D. Sampson, *At. Data Nucl. Data Tables* **43**, 1 (1989).
- [86] U. I. Safronova, C. Namba, I. Murakami, W. R. Johnson, and M. S. Safronova, *Phys. Rev. A* **64**, 012507 (2001).
- [87] C. Dong, L. Xie, S. Fritzsche, and T. Kato, *Nucl. Instrum. Methods Phys. Res., Sect. B* **205**, 87 (2003).
- [88] P. Jönsson, P. Bengtsson, J. Ekman, S. Gustafsson, L. B. Karlsson, G. Gaigalas, C. F. Fischer, D. Kato, I. Murakami, H. A. Sakaue, H. Hara, T. Watanabe, N. Nakamura, and N. Yamamoto, *At. Data Nucl. Data Tables* **100**, 1 (2014).
- [89] J. A. Santana, J. K. Lepson, E. Träbert, and P. Beiersdorfer, *Phys. Rev. A* **91**, 012502 (2015).
- [90] C. Cheung, M. Safronova, and S. Porsev, *Symmetry* **13**, 621 (2021).
- [91] M. F. Gu, *Can. J. Phys.* **86**, 675 (2008).
- [92] A. Kramida, Yu. Ralchenko, J. Reader, and NIST ASD Team, NIST Atomic Spectra Database, version 5.9, <https://physics.nist.gov/asd>.
- [93] A. R. Foster, L. Ji, R. K. Smith, and N. S. Brickhouse, *Astrophys. J.* **756**, 128 (2012).
- [94] G. Del Zanna and Y. Ishikawa, *Astron. Astrophys.* **508**, 1517 (2009).
- [95] J. S. Kaastra, R. Mewe, and H. Nieuwenhuijzen, in *11th Colloq. on UV and X-ray Spectroscopy of Astrophysical and Laboratory Plasmas*, edited by K. Yamashita and T. Watanabe (Universal Academy Press, Tokyo, 1996), pp. 411–414.
- [96] N. M. Cann and A. J. Thakkar, *Phys. Rev. A* **46**, 5397 (1992).
- [97] W. R. Johnson, I. M. Savukov, U. I. Safronova, and A. Dalgarno, *Astrophys. J. Suppl. Ser.* **141**, 543 (2002).
- [98] N. Werner, I. Zhuravleva, E. Churazov, A. Simionescu, S. W. Allen, W. Forman, C. Jones, and J. Kaastra, *Mon. Not. R. Astron. Soc.* **398**, 23 (2009).
- [99] M. Tashiro *et al.*, *Proc. SPIE* **10699**, 1069922 (2018).
- [100] F. Pajot *et al.*, *J. Low Temp. Phys.* **193**, 901 (2018).
- [101] R. Kraft *et al.*, [arXiv:2211.09827](https://arxiv.org/abs/2211.09827).
- [102] W. Cui, L. B. Chen, B. Gao, F. L. Guo, H. Jin, G. L. Wang, L. Wang, J. J. Wang, W. Wang, Z. S. Wang, Z. Wang, F. Yuan, and W. Zhang, *J. Low Temp. Phys.* **199**, 502 (2020).
- [103] R. K. Heilmann, A. R. Bruccoleri, V. Burwitz, C. DeRoo, A. Garner, H. M. Günther, E. M. Gullikson, G. Hartner, E. Hertz, A. Langmeier, T. Müller, S. Rukdee, T. Schmidt, R. K. Smith, and M. L. Schattenburg, *Astrophys. J.* **934**, 171 (2022).
- [104] F. Nicastro *et al.*, *Exp. Astron.* **51**, 1013 (2021).
- [105] D. A. Schwartz, A. Vikhlinin, H. Tananbaum, M. Freeman, G. Tremblay, E. D. Schwartz, J. A. Gaskin, D. Swartz, K. Gelmis, K. S. McCarley, and A. Dominguez, *SPIE Proc.* **11118**, 111180K (2019).
- [106] A. Kramida (personal communication) (2019).
- [107] I. I. Tupitsyn, M. G. Kozlov, M. S. Safronova, V. M. Shabaev, and V. A. Dzuba, *Phys. Rev. Lett.* **117**, 253001 (2016).